Dielectric relaxation in laser ablated polycrystalline $ZrTiO_4$ thin films

P. Victor, S. Bhattacharyya, and S. B. Krupanidhi[a)]
Materials Research Center, Indian Institute of Science, Bangalore 560 012, India

Relaxation and conduction mechanisms under small ac fields of laser ablated $ZrTiO_4$ thin films were analyzed in the light of impedance and modulus spectroscopy. The overall dielectric properties were mainly dominated by a Maxwell–Wagner type of relaxation with grains and the grain boundary two distinct parts of the circuit. Each of these parts was found to follow the universal power law of frequency dispersion. The modulus plot confirmed that the capacitive parts were relatively independent of the frequency and temperature, whereas the impedance and ac conduction studies exhibited significant temperature and frequency dependence. The conduction inside the grains was suggestive of a hopping mechanism through various defect sites whereas the interface barrier potential dictated grain boundary conduction.

I. INTRODUCTION

Recently there had been extensive investigation of linear dielectrics and ferroelectric materials for their use in dynamic random access memories (DRAMs),[1] gate dielectrics,[2] and microwave communications.[3] There is a continuing trend to scale down devices to smaller dimensions. The use of low dielectric constant materials has been eliminated since it limits reduction of the dimensions of thin films. In the case of such reduced dimension thin films, the existence of stronger electric fields eventually alters and degrades the device performance. Hence a serious issue has been considered to develop a new class of materials with higher dielectric constants and lower leakage currents. Recently perovskite materials, such as $(Ba,Sr)TiO_3$, $SrTiO_3$ thin films[4,5] and linear dielectrics like ZrO_2,[6] TiO_2,[7] Ta_2O_5,[8] $ZrTiO_4$, and $Zr(Sn,Ti)O_4$,[9] have been extensively investigated in this regard. Most of these materials are useful in gate dielectrics and microwave applications due to their higher dielectric constant, higher Q factor, and lower temperature coefficient of resonance. Van Dover *et al.*[10] have identified amorphous Zr–Sn–Ti–O as the most likely candidate for the DRAM applications because of its higher dielectric constant, lower leakage current, and higher dielectric breakdown strength. $ZrTiO_4$ (denoted ZT) and $(Zr,Sn)TiO_4$ thin films have found extensive usage in mobile communications in the form of phase shifters, voltage tunable oscillators, and filters.[11] They are widely used in satellite communications because of their higher dielectric constant in the microwave frequency regime and almost zero temperature coefficient of resonance. ZT thin films were deposited using different deposition techniques including rf and dc magnetron sputtering,[12,13] sol–gel[14] and pulsed laser ablation techniques.[15] The pulsed laser ablation technique is suitable for depositing multicomponent oxides and has the advantage of maintaining excellent stoichiometry of the target on thin films.

$ZrTiO_4$ is α-PbO type, with orthorhombic symmetry and a $Pbcn$ space group with the Zr^{4+} and Ti^{4+} cations distributed randomly within the lattice.[16] ZT has an incommensurate phase (IC) and is known to decrease the quality factor in comparison to normal and constant phases. It undergoes a second-order phase transition from N phase to the structurally IC modulated phase at 1125 °C with a first-order transition at 845 °C.[17] Recently we conducted a thorough analysis of laser ablated ZT thin films on a Si substrate in a metal–oxide–semiconductor (MOS) configuration, and it exhibited excellent thermal stability and lattice match on Si, which are essential in ultralarge scale integrated (ULSI) devices.[18] In this article, we present the results and analysis of dielectric relaxation observed in polycrystalline ZT thin films deposited on a Pt coated Si substrate in a metal–insulator–metal (MIM) configuration.

II. EXPERIMENT

A single phase dense $ZrTiO_4$ target was prepared via a conventional solid-state reaction method by mixing and calcining the multicomponent oxides at 1450 °C for 6 h and then the powders were pressed into a 12 mm pellet. The pressed pellet was sintered at 1550 °C for 6 h to form a single phase ZT target. The ZT target was used for ablation and the thin films were deposited on a Pt (111) coated Si substrate by a KrF (248 nm) pulsed excimer laser. The substrate temperatures ranged from 300 to 650 °C at varied operating pressures from 5 to 100 mTorr in pure oxygen ambient. The thickness of the ZT thin films was in the range of 250–500 nm, measured using an optical thin film thickness measuring system (FILMETRICS). Structural phase determination was performed using an x-ray diffractometer (Scintag XR2000) and the grain morphology was examined by a scanning electron microscope. The uniformity in the distribution of the elements in the thin films and substrate–thin film interface was studied by secondary ion mass spectrometer (SIMS). Gold dots of 1.96×10^{-3} cm^2 area were deposited by thermal evaporation onto the ZT thin films as top elec-

[a)]Author to whom correspondence should be addressed; electronic mail: sbk@mrc.iisc.ernet.in

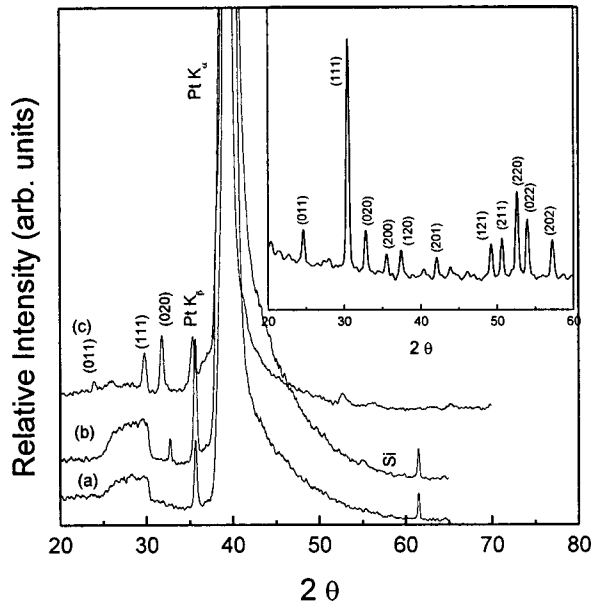

FIG. 1. X-ray diffraction of $ZrTiO_4$ thin films at different temperatures. The inset shows the powder XRD of the $ZrTiO_4$ target.

trodes in a metal–insulator–metal (Au/ZT/Pt) configuration to carry out the electrical measurement. The electrodes were annealed at 350 °C for 10 min. A Keithley LCZ 3330 system coupled with Keithley SMU 236 was used for conventional dielectric and $C-V$ measurements. All electrical measurements of the ZT thin films were carried at different temperatures between 30 and 250 °C.

III. RESULTS AND DISCUSSION

A. Structural determination

Confirmation of phase formation was made by the x-ray diffraction pattern as shown in Fig. 1. The deposition temperature was found to play an important role in the phase evolution process, as shown in Fig. 1. The samples showed an almost amorphous nature when deposited at low temperatures and, as the temperature was increased, the sample assumed a polycrystalline structure. From this study, the optimum temperature was found to be 625 °C. Three main peaks confirmed the phase in the sample, and they were the 111, 020, and 022 peaks. There was an amorphous background in the vicinity of the 111 peak at lower temperature, which suggested that, in the initial stages, there might have been some amorphous phase present in the sample. This amorphous phase disappeared at higher substrate temperatures. Incidentally the 020 peak overlapped the silicon 200 peak position (which even though forbidden appears occasionally), but the systematic evolution of this particular peak with the deposition temperature confirmed this peak could be attributed to the sample.

B. Dielectric studies

Figures 2(a) and 2(b) represent the dispersion curves of the dielectric constant and the loss tangent, respectively, at different temperatures. The real part of the dielectric constant exhibited rolloff at frequency in the range of 100–1000 Hz at room temperature, with a loss peak accompanying it. The loss peak showed a continuous trend of shifting towards high frequencies at high temperatures; at temperatures higher than 200 °C, the loss peak was out of the frequency window of measurement. The peak was preceded by an initial decrease, which was inversely proportional to the frequency. This decrease of the loss factor with frequency was observed only at the low frequency range (0.1–1 kHz), and this range was extended with the temperature. No significant change was detected in the width of the peak with the temperature.

The negative slope of the low frequency dispersion curve suggested a conduction-dominated loss at low frequency through a parallel RC circuit (assuming the system to be homogeneous):

$$\tan\delta = 1/\omega CR. \tag{1}$$

This is true, provided both the capacitance and the resistive elements are frequency independent (at least at low frequencies). We have also observed that, ''rolloff'' in the dielectric constant occurred through a wide range of frequency and, consequently, the loss peak also covered the same frequency range. Therefore, even at frequencies well below the loss peak frequency, a decreasing trend was observed in the capacitance and, therefore, the capacitance (C) in Eq. (1) could not be regarded as a constant anymore. We have therefore plotted $C\times\tan\delta$ (which is basically the imaginary part of the complex capacitance) as a function of ω [Fig. 2(c)]. When the slope of the $\epsilon''\sim\omega$ curve was calculated for a temperature of 225 °C, it yielded a value of -0.91. The deviation from unity could have resulted from a low frequency ''space-charge'' effect among the grains/grain boundaries, which caused inverse frequency dependence of the resistance also. This was also confirmed from an ac conductivity plot, since the conductivity (which is the inverse of resistivity) exhibited low frequency dispersion (at 225 °C) of the form

$$\sigma\propto\omega^{0.08}.$$

The inverse frequency dependence of the imaginary dielectric constant at low frequencies was confirmation of the non-Debye type character of the overall relaxation. In Debye type relaxation, the loss factor should start from a zero value at zero frequency, and then should show a proportional relationship with the frequency according to

$$\tan\delta = \omega CR, \tag{2}$$

which is basically equivalent to a series combination of a resistive with a capacitive component. It was therefore seen that the overall dielectric relaxation was not explainable by either of these two mechanisms, since the imaginary capacitance was in accordance with conduction loss at low frequencies, while at intermediate frequencies, the loss peak was suggestive of a different possibility. It was thought that the dielectric dispersion was not explainable by assuming the system to be homogeneous, instead, there might have been more than one region which individually contributed to the dielectric response. One possible combination could be the usual grain and grain boundary (series) combination, each region being a parallel combination of capacitance and resistance. This is the equivalent to Maxwell–Wagner type relax-

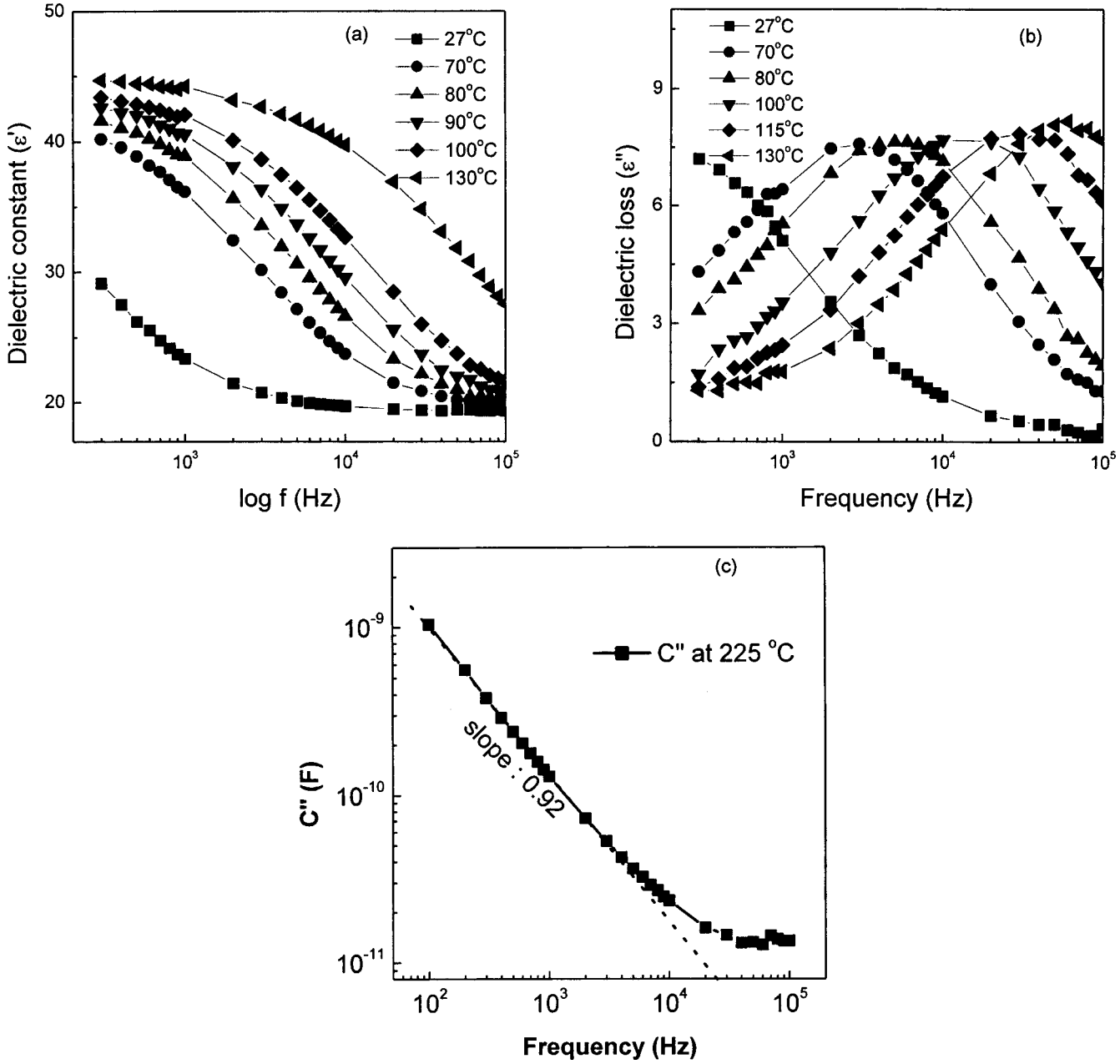

FIG. 2. (a) Dielectric constant vs the frequency at different temperatures. (b) Dielectric loss vs the frequency at different temperatures. (c) Low frequency dispersion of the imaginary dielectric constant at 225 °C.

ation, where additional capacitance comes from extrinsic sources such as grain/grain-boundary charge accumulation. The peak approximately corresponds to a situation where the grains contribute mainly to the resistance and the grain boundary contributes only to the capacitive effect. Essentially, this becomes a series resistance–capacitance (RC) circuit at that frequency range (when the grain boundary capacitance dominates the impedance of the grain boundary, but the grain impedance is still governed by the resistance of the grains). However, this approximation might not hold very well in a real case, hence it might be misleading to take the loss peak frequency for any quantitative calculations, for instance, the activation energy for hopping, or such.

On the other hand, the impedance diagram can be much more informative, since it can decouple grain and grain boundary effects, and give the true grain resistance. Impedance spectroscopy has been quite well known for its applications in solid electrolyte conductivity determination,[19] and its use has also long been extended to the studies of other solid dielectrics. Any real ceramic material or thin film can be thought of as consisting of mainly two dissimilar regions, namely, the grain and the grain boundary. Each region can be realistically described by a parallel combination of a capacitor and a resistor. There can be differences in the capacitance and resistance values between different grains because of slight differences in shape. The size effect should not affect too much in first order, because, in most of the cases, the calculations would deduce down to the functions of CR, which is essentially independent of the size of a regular rectangular slab. Therefore, one could assume a distribution of

resistance (or RC time constants), but it should never be so broad that it overlaps the relaxation time of the other region. The complex impedance Z^* can be expressed in the following way:

$$Z^* = R(1 - j\omega\tau)/(1 + \omega^2\tau^2), \tag{3}$$

where R and C are, respectively, the resistance and capacitance of the parallel circuit. In a real case, there would be a distribution in the relaxation time, and also the resistance and capacitance would be slightly frequency dependent. The modified expression for Z in such a case would be equivalent to the Cole–Davidson relation:[20]

$$Z^* = R(1 - j\omega\tau)/[1 + (\omega\tau)^{1-\alpha}], \tag{4}$$

where τ is the average relaxation time, and α characterizes the distribution of the relaxation time. One can observe that the imaginary part of the impedance would pass through a maximum in the spectroscopic plot, and this maximum would correspond to a situation where $\omega\tau = 1$, and the maximum value of Z_{Im} would be given by

$$Z_{\mathrm{Im}}(\max) = R/2. \tag{5}$$

The values of R in a correlated charge carrier system are a frequency dependent parameter. In perovskite oxides or in many other ionic solid materials, the major mode of charge transport is a multiple hopping process.[21] The hopping process normally takes place across the potential barriers set up by the lattice structure and the local environment of other atoms/ions. However, due to irregularities in the lattice structure near defect sites, the potential barriers will have different magnitudes, as well as varied widths.[22,23] This is thought to be responsible for the distribution in the relaxation times.

The other theory explains the conduction through ionic solids/glasses by assuming a highly disordered medium and close interaction between the charge carriers themselves.[24,25] Irrespective of what the microscopic mechanism behind the motion of the charge carriers is, the final frequency dependence of macroscopic resistance R_{ac} (which is just the inverse of ac conductivity) in such cases can be written as

$$R_{\mathrm{ac}} \propto \omega^{-n}, \tag{6}$$

where $0 < n < 1$. Therefore, as explained in Fig. 2, the maxima in the Z_{Im} plot should appear at a higher frequency than $\omega = 1/\tau$.

Figure 3 shows the imaginary impedance as a function of the frequency. The peak shifted towards higher frequencies as the temperature increased. The magnitude of the imaginary component of the impedance at the peak frequency was also a strongly varying function of the temperature, indicating Arrhenius type temperature dependence. This result can be seen in the Arrhenius plot of the peak frequency in the impedance plot (Fig. 4), which was fairly linear at high temperature. The corresponding activation energy was 0.56 eV, indicating oxygen vacancy controlled conduction. The width of the peak was 1.28 decade, confirming non-Debye type (where the peak width should be 1.14 decade) relaxation. In the frequency window of our measurement, we could observe only one peak, which certainly represented the grain contribution, whereas the grain boundary contribution

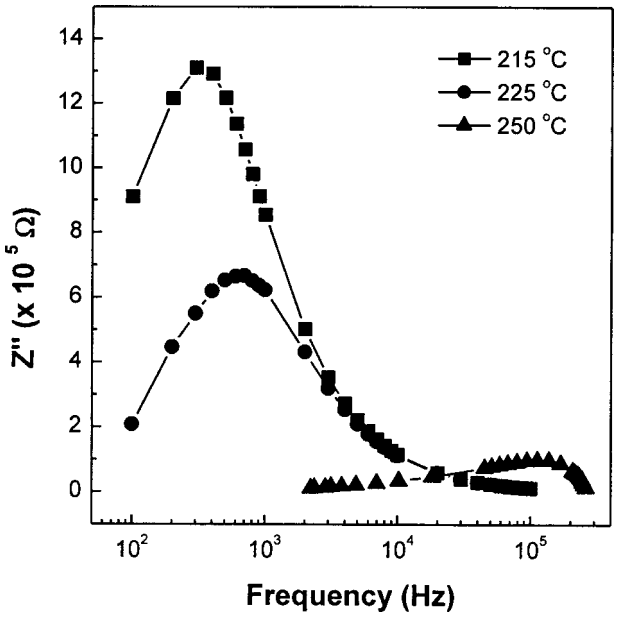

FIG. 3. Imaginary impedance with frequency at different temperatures.

appeared at much higher temperature, and at much lower frequencies. Figure 5 shows the impedance plot at different temperatures in the complex representation. At higher temperature, one can vividly observe a good fit of this curve, with the generated equation of a semicircle. The center of the fitted semicircle (with the impedance plot) was lying slightly below the abscissa proving departure from the pure Debye nature, and confirming Jonscher universal frequency dependence. The inclination of the semicircle with respect to the real axis increased with the temperature, indicating that departure from the Debye nature was partly thermally assisted. The value of the angle of deviation (from the real axis) was calculated by drawing a tangent to the high frequency end of

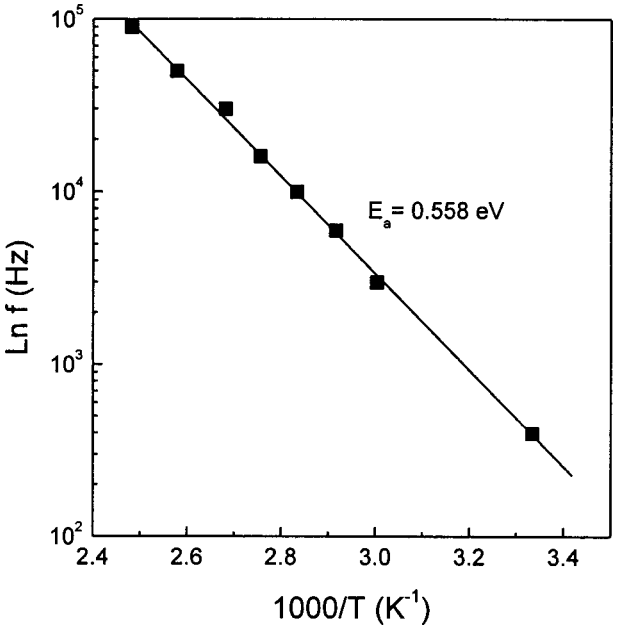

FIG. 4. Arhennius plot of the peak frequencies obtained from the imaginary part of the impedance.

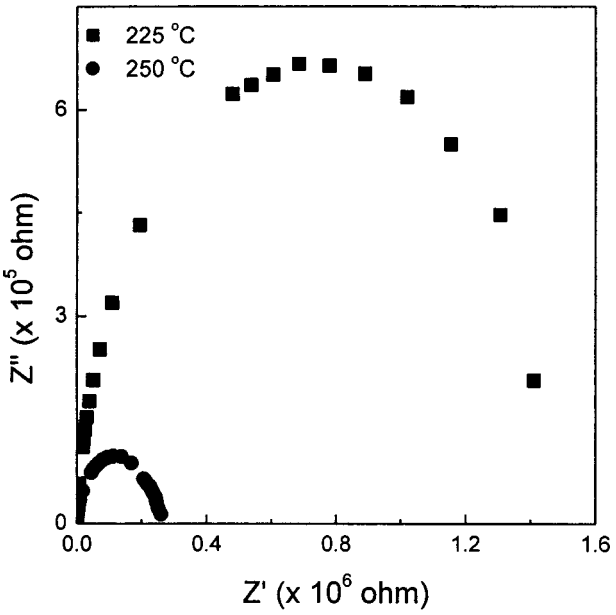

FIG. 5. Complex impedance plot of $ZrTiO_4$ thin films.

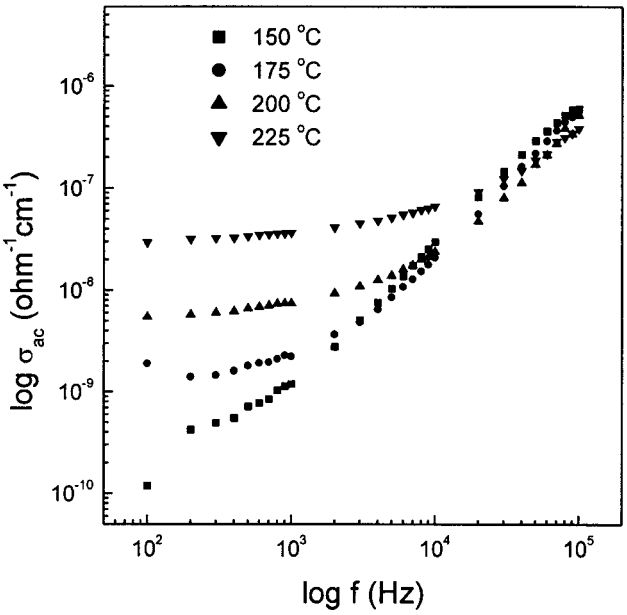

FIG. 6. Plot of the ac conductivity at different temperatures.

the first semicircle (which represented the grain). The angle between the tangent and the imaginary axis was the same as the angle between the diameter of the circle and the real axis. According to Jonscher's law,[25] the deviation angle is directly related to exponent n through the equation

$$\Delta\theta=(1-n)\pi/2. \tag{7}$$

At high temperature, there was also another deviation from the circular nature observed at the low frequency side of the complex impedance plot. This was possibly the result of the grain boundary contribution, due to its high resistance and high capacitance, the associated time period was longer, and all the grain boundary contribution was visible only at low frequencies. The high frequency side originated from the grains, and was in fairly good agreement with the equation of a generated semicircle. The high temperature and low frequency tail were not fully evolved to its true shape because of frequency and temperature limitations. However, it is known that the grains and grain boundaries have a huge difference (orders of magnitude) in respective resistance values, and the impedance plot is essentially governed by the resistive part [Eq. (5)] only. It is therefore difficult to obtain two full circles (representing grains and grain boundary) on the same scale in the impedance plot.

The power law behavior of the resistance and also of the capacitance was directly reflected in the ac conductivity plot shown in Fig. 6. The following equation was used to calculate the ac conductivity of the system:[21]

$$\sigma=\epsilon_0\epsilon\omega\tan\delta. \tag{8}$$

From the curve it was evident that, at low frequencies, the ac conductivity was almost frequency independent, which was representative of dc leakage current throughout the sample, and was only dependent upon the voltage applied. At higher frequencies, the ac conductivity increased, since the response from the transient regime was also included. The inverse power law time dependence of the transient current confirmed Curie–von Schweideler theory,[26] and indicated an interacting dipole/charge carrier system. However, this was observed only in the transient regime, and that is why the power law was more prominent at the high frequency range. In the intermediate frequency regime, exponent n itself was also a function of the frequency. Due to the exponential increase in the dc leakage current with the temperature the frequency independent conductivity region was also extended towards higher frequencies. The value of n was reduced at higher temperatures, indicating an increase in the randomness in the system, which made the dipoles (and also the charge carriers) respond independently of each other to the external field.

At the very beginning of the ac conductivity plot at room temperature, the slope was slightly more than unity, which was followed by a much more slowly varying conductivity. Power law behavior was observed at the high frequency limit. A careful investigation of the expression for the ac conductivity reveals that the conductivity is a product of the frequency and the imaginary part of the dielectric constant and, therefore, a greater than unity slope of the log σ vs log ω curve indicated an increase of ϵ'' with the frequency. This indicated that a loss peak was approaching. The loss peak corresponded to the crossover from grain contribution to grain boundary contribution. We observed the loss peak at the beginning of the frequency spectrum at room temperature, but as the temperature was raised, the loss peak shifted towards higher frequencies, indicating that the grain boundary effects were dominating the frequency response of ac conductivity over the entire range. The overall conductivity plot was therefore thought of as consisting of two segments, representing the grains and grain boundary, respectively, with each segment obeying power law dependence on the frequency. Identical behavior in fine-grained $SrTiO_3$ ceramic was predicted and also experimentally verified by Waser and co-workers.[27] In that report, they showed that there existed two horizontal parts of the ac conductivity, which basically

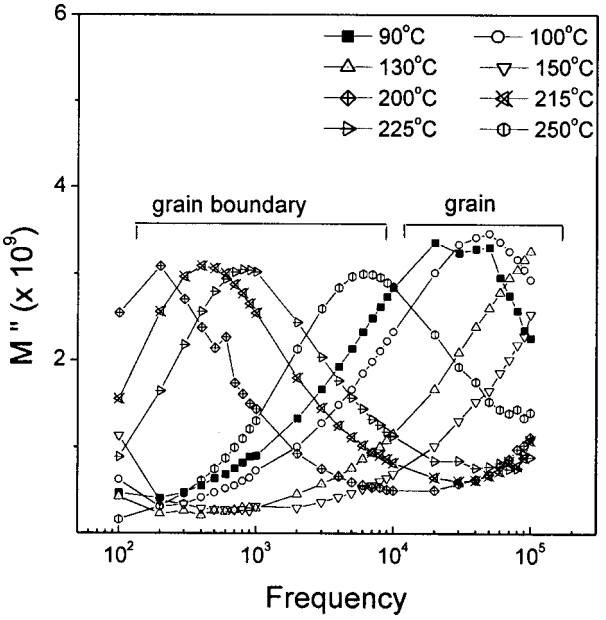

FIG. 7. Plot of the imaginary electric modulus at various temperatures.

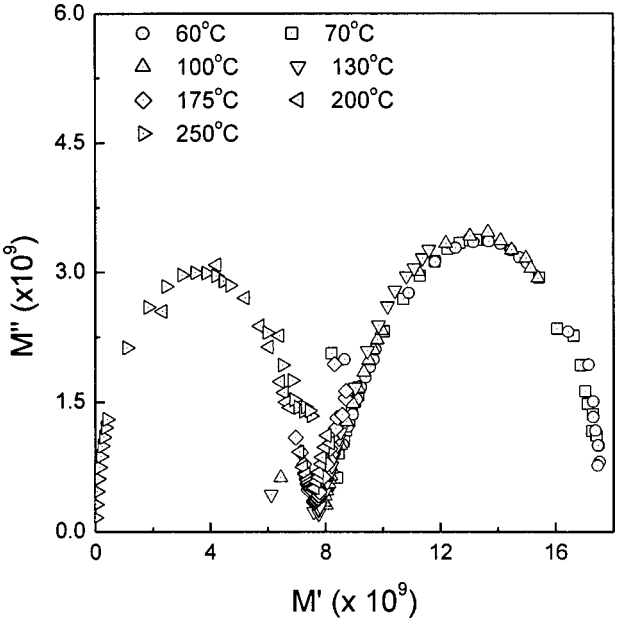

FIG. 8. Plot of the complex electric modulus of $ZrTiO_4$ thin films.

represented the dc conductivities of these two regions of the total circuit.

In the impedance plot, we could not clearly resolve more than one semicircle because of the frequency window limitation. It is known that when there is a large difference in the resistance of two dissimilar regions, the two semicircles in the complex impedance plot would also vary in size by orders of magnitude. It would, therefore, be difficult to observe two distinct semicircles in the complex impedance plot. However, if the electric modulus of the same system is calculated, then the modulus plot would highlight the effect of capacitance in these two regions.[28] If the capacitances are of comparable value (even though the resistance might vary by orders of magnitude), one can expect two distinct semicircles in the modulus plot calculated from the same set of data. The electric modulus was calculated from the following equation:

$$M^* = C_0 j\omega Z^* \tag{9}$$

Figure 7 shows the imaginary modulus as a function of the frequency at different temperatures. We have noticed two maxima in the spectroscopic plot, but the frequency limitation restricted to observe both the curves at the same temperature. However, both these peak frequencies exhibited shifts upward with the temperature, and hence it was possible to capture both these peaks in the same frequency window, but at different temperatures. The same effect was also reflected in the complex modulus plot (Fig. 8), where we noticed the presence of two distinct semicircles. The first semicircle was thought to represent the grain boundary, and the second one the grains. The intersection of the first semicircle with the abscissa showed the inverse of the grain boundary capacitance, and the second one the inverse of the total (series) capacitance. It was found that, even though the complex modulus plots covered different parts of a double circle, when they were plotted on the same scale (as that in Fig. 8), all the curves fit a single master curve. This indicted that the major temperature dependence of the ac electrical properties of the overall system was due to the change in resistance of the grains and the grain boundaries while the capacitance values remained more or less independent of the temperature. It also reflected the fact that both the grain boundary and the grains had comparable capacitance values. When the imaginary parts of both the impedance and the modulus of the grain were plotted [Fig. 9(a)], one could see that there was a difference in peak frequency observed in Z^* and M^*. This behavior suggested possible inherent frequency dependence of the capacitance and the resistance. Combining Eqs. (4) and (9), one gets the following expression for M^*:

$$M^* = C_0[\omega\tau/(1+(\omega\tau)^{1-\alpha})]1/C. \tag{10}$$

For a distributed relaxation process, capacitance C can also be expressed as

$$C \propto \omega^{1-n}.$$

The expression for the modulus therefore becomes equal to the second term in Eq. (4) multiplied by a factor of ω^{1-n}. The ω^{1-n} term increases with the frequency, shifting the modulus peak upward in the spectroscopic plot.

In our case, we have noticed that the modulus plots for all the temperatures fell on different parts of the same master curve, so we could conclude that the inherent frequency dependence was mainly due to the resistance rather than to the capacitance. Therefore, we normalized only the impedance by an expression, ω^{-n} [according to Eqs. (4) and (6)], and replotted the impedance [Fig. 9(b)]. One can see that, after this normalization, both the impedance and modulus peaks occurred at the same frequencies.

We have demonstrated that the capacitance of neither the grain nor the grain-boundary changed appreciably with the temperature. It was only the resistance of the grains/grain boundaries, which were functions of the temperature in the

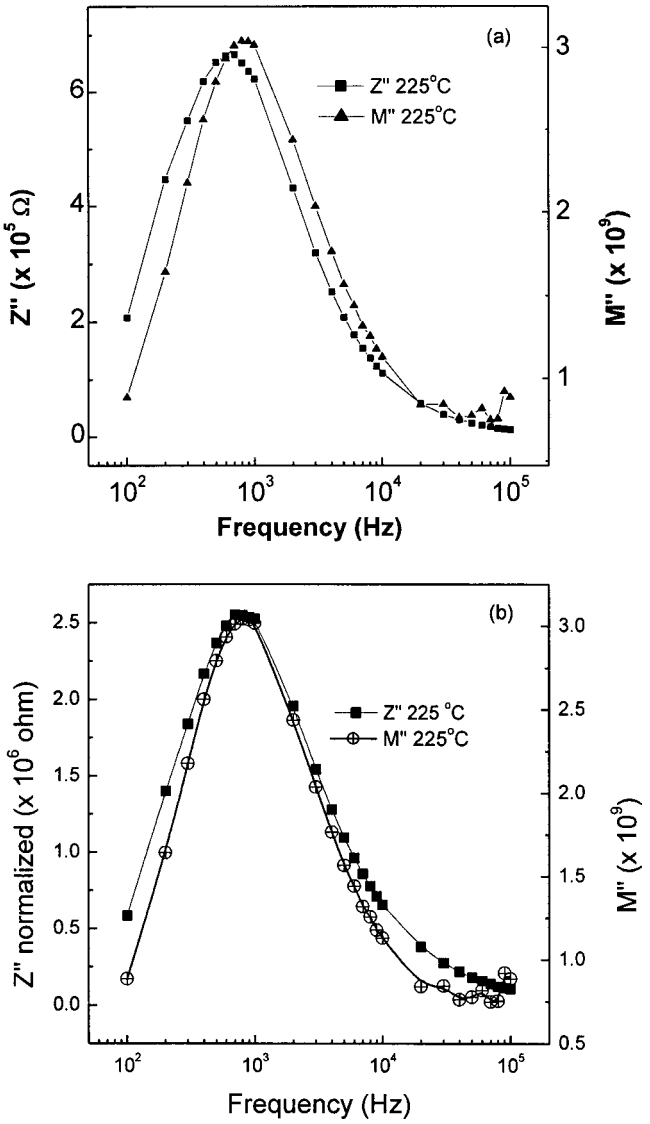

FIG. 9. (a) Imaginary part of the impedance and modulus vs the frequency measured at 225 °C. (b) Normalized imaginary part of the impedance and modulus vs the frequency at 225 °C.

expression for the modulus peak frequencies. Hence one could associate the Arrhenius equation with the peak frequencies. Figure 10 displays the Arrhenius plot of the low and high frequency peaks. The high frequency peak revealed an activation energy of 0.52 eV whereas the low frequency peak had an activation energy of 1.32 eV. The low frequency peak was from grain boundary contributions, and the observed activation energy values suggested that the grain boundaries required higher activation energies for hopping across them than the grains. This indicated possible grain boundary barrier formation against electron conduction. It was likely that the conduction through the grain boundary was the motion of electrons, since ionic motion across the grain boundary might be easier than the more tightly packed grains. Inside the grains, the low value for the activation energy was suggestive of either the electron being trapped in shallow potential wells or oxygen vacancies. Our conclusion was, therefore, that inside the grains, both electrons and oxygen vacancies dominated the conduction, and electronic conduction was the major contributor in the grain boundary regions.

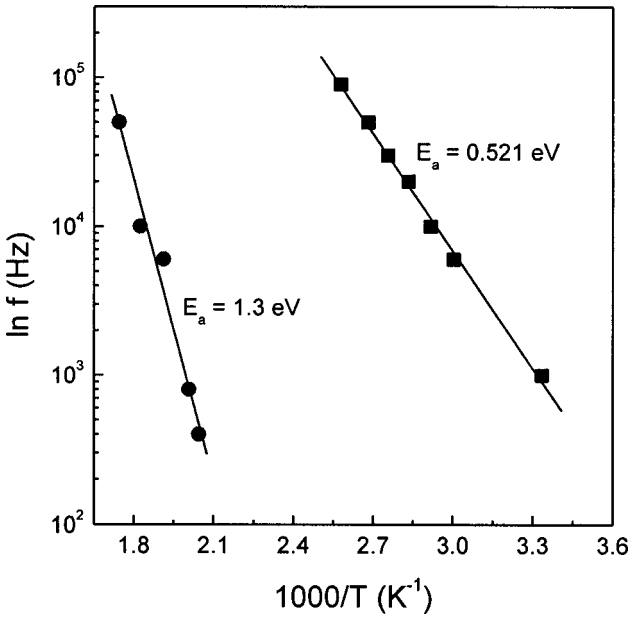

FIG. 10. Arrhenius plot obtained from the complex electric modulus spectra (M' vs M'').

IV. CONCLUSIONS

We have analyzed the dielectric and ac conduction behavior of polycrystalline thin $ZrTiO_4$ films. It was found that the overall dielectric properties were governed by Maxwell–Wagner type relaxation, but the relaxation suggested that both the grains and grain boundary had inherent frequency dispersion. From the ac conductivity plot, we saw that the ac resistance really showed universal power law dependence according to the Jonscher model. The impedance plot showed a tilted semicircle, confirming the validity of the Jonscher model. In the electric modulus plot, the existence of two distinct semicircles was clearly evident. The shapes of the modulus plots at different temperatures were almost the same, and this indicated that the capacitive components were independent of the temperature and also of the frequency, since the frequency dependence is also affected by the temperature. The inherent frequency dependence was believed to have originated from the resistive parts only. The impedance and the modulus peaks showed a difference in peak frequency as a consequence of this inherent frequency dependence of the resistive elements. After normalizing the imaginary impedance, both the impedance and the modulus peaks were found to occur in the same frequency regime.

ACKNOWLEDGMENT

One of the authors (P.V.) wishes to acknowledge the Council for Scientific and Industrial Research, India, for a graduate fellowship.

[1] K. S. Tang, W. S. Lau, and G. S. Samudra, IEEE Circuits Devices Mag. **13**, 27 (1997).
[2] G. D. Wilk, R. M. Wallace, and J. M. Anthony, J. Appl. Phys. **89**, 5243 (2001).

[3] K. Wakino, T. Nishikawa, Y. Ishikawa, and H. Tamura, Br. Ceram. Trans. J. **89**, 39 (1990).
[4] H. Takagi, N. Fujinami, H. Tamura, and K. Wakino, Jpn. J. Appl. Phys., Part 1 **31**, 3269 (1992).
[5] P. Bhattacharya, T. Komeda, K. Park, and Y. Nishioka, Jpn. J. Appl. Phys., Part 1 **32**, 4103 (1993).
[6] M. Copel, M. Gribelyyuk, and E. Gusev, Appl. Phys. Lett. **76**, 436 (2000).
[7] S. A. Campbell, H. S. Kim, D. C. Gilmer, B. He, T. Ma, and W. L. Gladfelter, IBM J. Res. Dev. **43**, 383 (1999).
[8] P. K. Roy and I. C. Kizlilyalli, Appl. Phys. Lett. **72**, 2835 (1998).
[9] H. Tamura, Am. Ceram. Soc. Bull. **73**, 93 (1994).
[10] R. B. Van Dover, L. F. Schneemeyer, and R. M. Fleming, Nature (London) **392**, 162 (1998).
[11] G. Wolfram and E. Gobel, MRS Bull. **16**, 1455 (1981).
[12] D.-A. Chang, P. Lin, and T.-Y. Tseng, J. Appl. Phys. **78**, 7103 (1995).
[13] T. Kim, J. Oh, B. Park, and K. S. Hong, Jpn. J. Appl. Phys., Part 1 **39**, 4153 (2000).
[14] V. Bornand, P. Papet, and E. Philippot, J. Mater. Sci. Lett. **18**, 483 (1999).
[15] O. Nakagawara, Y. Toyota, M. Kobayashi, Y. Yoshino, Y. Katayama, H. Tabata, and T. Kawai, J. Appl. Phys. **80**, 388 (1996).
[16] R. E. Newnham, J. Am. Ceram. Soc. **50**, 216 (1967).
[17] R. Christoffersen, P. K. Davies, and X. Wei, J. Am. Ceram. Soc. **77**, 1441 (1994).
[18] P. Victor, J. Nagaraju, and S. B. Krupanidhi, Proceedings of IEEE, ISAF 2002, p. 207, IEEE Catalogue No. 207.
[19] J. R. McDonald, *Impedance Spectroscopy* (Wiley, New York, 1987).
[20] D. W. Davidson and R. H. Cole, J. Chem. Phys. **19**, 1484 (1951).
[21] V. Gupta and A. Mansingh, Phys. Rev. B **49**, 1989 (1994).
[22] H. Kliem, IEEE Trans. Electr. Insul. **24**, 185 (1989).
[23] R. Waser, *Science and Technology of Electroceramic Thin Films* (Kluwer Academic, Dordrecht, The Netherlands, 1995).
[24] N. F. Mott and E. A. Davis, *Electronic Processes in Non-crystalline Materials*, 2nd ed. (Clarendon, Oxford, 1979).
[25] A. K. Jonscher, *Dielectric Relaxation in Solids* (Chelsea Dielectric, London, 1983).
[26] E. von Schweidler, Ann. Phys. (Leipzig) **24**, 711 (1907).
[27] M. Vollmann, R. Hagenbeck, and R. Waser, J. Am. Ceram. Soc. **80**, 2301 (1997).
[28] I. M. Hogde, M. D. Ingram, and A. R. West, J. Electroanal. Chem. Interfacial Electrochem. **58**, 429 (1975).